

Experimental study of turbulent transport of nanoparticles in convective turbulence

Cite as: Phys. Fluids **34**, 055126 (2022); <https://doi.org/10.1063/5.0087873>

Submitted: 10 February 2022 • Accepted: 06 May 2022 • Accepted Manuscript Online: 07 May 2022 • Published Online: 23 May 2022

I. Shimberg,  O. Shriki, O. Shildkrot, et al.



View Online



Export Citation



CrossMark

ARTICLES YOU MAY BE INTERESTED IN

[Experimental study of turbulent thermal diffusion of particles in inhomogeneous and anisotropic turbulence](#)

Phys. Fluids **34**, 055125 (2022); <https://doi.org/10.1063/5.0088982>

[Effects of wing-body interaction on Hawk-moth aerodynamics and energetics at various flight velocities](#)

Phys. Fluids (2022); <https://doi.org/10.1063/5.0087161>

[Turbulent channel flow of a binary mixture of neutrally buoyant ellipsoidal particles](#)

Phys. Fluids **34**, 053609 (2022); <https://doi.org/10.1063/5.0089088>

LEARN MORE

APL Machine Learning

Open, quality research for the networking communities

MEET OUR NEW EDITOR-IN-CHIEF



Experimental study of turbulent transport of nanoparticles in convective turbulence

Cite as: Phys. Fluids **34**, 055126 (2022); doi: [10.1063/5.0087873](https://doi.org/10.1063/5.0087873)

Submitted: 10 February 2022 · Accepted: 6 May 2022 ·

Published Online: 23 May 2022



View Online



Export Citation



CrossMark

I. Shimberg, O. Shriki,  O. Shildkrot, N. Kleorin,  A. Levy,  and I. Rogachevskii^{a)} 

AFFILIATIONS

The Pearlstone Center for Aeronautical Engineering Studies, Department of Mechanical Engineering, Ben-Gurion University of the Negev, P.O. Box 653, Beer-Sheva 8410530, Israel

^{a)} Author to whom correspondence should be addressed: gary@bgu.ac.il

ABSTRACT

We perform an experimental study of transport of nanoparticles in convective turbulence with the Rayleigh number $\sim 10^8$ in the air flow. We measure a temperature field in many locations by a temperature probe equipped with 11 E-thermocouples. Nanoparticles of the size ~ 70 nm in diameter are produced by an advanced electrospray aerosol generator. To determine the number density of nanoparticles, we use a condensation particle counter. The joint action of turbulent effects and the large-scale circulations in convective turbulence, which are important in the core flow, and molecular effects, which are essential near the boundaries of the chamber, results in an effective accumulation of nanoparticles at the cold wall of the chamber. The turbulent effects are characterized by turbulent diffusion and turbulent thermal diffusion of nanoparticles, while the molecular effects are described by the Brownian diffusion and thermophoresis, as well as the adhesion of nanoparticles at the cold wall of the chamber. In different experiments in convective turbulence in a chamber with the temperature difference ΔT between the bottom and top walls varying between $\Delta T = 29$ and $\Delta T = 61$ K, we find that the mean number density of nanoparticles decreases exponentially in time. For instance, the characteristic decay time of the mean number density of nanoparticles varies from 12.8 min for $\Delta T = 61$ K to 24 min for $\Delta T = 29$ K. For better understanding of experimental results, we perform one-dimensional mean-field numerical simulations of the evolution of the mean number density of nanoparticles for conditions pertinent to the laboratory experiments. The obtained numerical results are in agreement with the experimental results.

Published under an exclusive license by AIP Publishing. <https://doi.org/10.1063/5.0087873>

I. INTRODUCTION

Turbulence^{1–7} and the associated turbulent transport of particles^{8–14} have been investigated systematically for more than a hundred years in theoretical, experimental, and numerical studies. However, some fundamental questions remain. It is well-known that turbulence results in a sharp increase in the effective diffusion coefficient.¹⁵ In addition to turbulent diffusion, there are various turbulent effects resulting in formation of inhomogeneities in the spatial distribution of particles.

In a non-stratified inhomogeneous turbulence, turbophoresis of particles due to a combined effect of particle inertia and inhomogeneity of turbulence can occur.^{16–21} Turbophoresis causes an appearance of the additional non-diffusive flux of inertial particles proportional to the mean particle velocity, $V_{\text{turbo}} \propto -f_{\text{turbo}}(\text{St}, \text{Re}) \nabla \langle \mathbf{u} \rangle^2$, where \mathbf{u} is the turbulent fluid velocity, $\text{St} = \tau_p / \tau_\eta$ is the Stokes number, $\tau_\eta = \tau_0 / \text{Re}^{1/2}$ is the Kolmogorov viscous time, $\tau_p = m_p / (3\pi\rho\nu d)$ is the Stokes time for the small spherical particles of the diameter d and mass m_p , ρ is the fluid density, $\text{Re} = \ell_0 u_0 / \nu$ is the fluid Reynolds

number, u_0 is the characteristic turbulent velocity at the integral scale ℓ_0 of turbulent motions, and ν is the kinematic fluid viscosity. Due to turbophoresis, inertial particles are accumulated in the vicinity of the minimum of the turbulent intensity.

In a turbulent flow with a non-zero mean temperature gradient, an additional turbulent flux of particles appears in the direction opposite to that of the mean temperature gradient.^{22,23} This phenomenon of turbulent thermal diffusion causes a non-diffusive turbulent flux of particles in the direction of the turbulent heat flux (opposite to the mean temperature gradient). Turbulent thermal diffusion results in accumulation of particles in the vicinity of the mean temperature minimum, which leads to the formation of inhomogeneous spatial distributions of the mean particle number density. Turbulent thermal diffusion has been intensively investigated analytically^{24–29} using different theoretical approaches. This phenomenon has been detected in laboratory experiments for micrometer-size particles in air flows in oscillating grid turbulence^{30–32} and in multi-fan produced turbulence.³³ Turbulent thermal diffusion has been also detected in direct

numerical simulations³⁴ and observed in the atmospheric turbulence.^{35,36} This phenomenon has been also shown to be important in astrophysical turbulent flows.³⁷

In spite of intensive laboratory studies of turbulent thermal diffusion of micrometer-size particles, this effect has not yet been investigated for nanoparticles. To study turbulent thermal diffusion of nanoparticles, one needs to take into account the dependence of the characteristic relaxation time of particles (the Stokes time) on the Knudsen number, $Kn = 2\lambda/d$,¹¹ where λ is the mean free path of molecules and d is the particle diameter. Note also that various aspects of transport of nanoparticles in turbulent fluid flows have been studied in a number of papers.^{38–46}

In the present paper, we discuss results of the experimental study of transport of nanoparticles in convective turbulence. The combined effects of turbulent thermal diffusion and the large-scale circulations in convective turbulence in the flow core, and molecular thermophoresis and adhesion of nanoparticles nearby the cold boundary, cause the accumulation of nanoparticles nearby the cold wall. Our main goal is to understand how fast it is possible to accumulate nanoparticles nearby the cold wall of the chamber and how to control this process. The effect of nanoparticle accumulation depends on properties of the temperature stratified turbulence. To understand how to control nanoparticle accumulation, we perform measurements of temperature fields in many locations in the chamber and conduct the direct measurements of the number density of nanoparticles in the chamber. This allows us to determine the time-dependence of the mean number density of nanoparticles in the chamber. To understand the experimental results, we also perform one-dimensional mean-field numerical simulations of transport of nanoparticles for conditions pertinent to the laboratory experiments.

This paper is organized as follows: In Sec. II, we discuss the physics of turbulent thermal diffusion, and in Sec. III, we outline the numerical setup for the mean-field numerical simulations of turbulent transport of nanoparticles. In Sec. IV, we describe the experimental setup and measurements techniques. In Sec. V, we discuss the experimental results and compare these results with those of the mean-field numerical simulations performed for conditions pertinent to the laboratory experiments. Finally, conclusions are drawn in Sec. VI.

II. TURBULENT THERMAL DIFFUSION

In this section, we discuss the physics of the phenomenon of turbulent thermal diffusion. The evolution of the number density $n(t, \mathbf{r})$ of small particles in a turbulent flow is determined by the convective diffusion equation

$$\frac{\partial n}{\partial t} + \mathbf{V} \cdot (n \mathbf{U}_p) = -\mathbf{V} \cdot \mathbf{J}_M, \quad (1)$$

where \mathbf{U}_p is the particle velocity advected by a turbulent temperature stratified fluid flow and \mathbf{J}_M is the molecular flux of particles that is given by

$$\mathbf{J}_M = -D \left[\mathbf{V}n + k_t \frac{\mathbf{V}T}{T} + k_p \frac{\mathbf{V}P}{P} \right], \quad (2)$$

where T and P are the temperature and pressure of the surrounding fluid, respectively. The first term ($\propto \mathbf{V}n$) in the right-hand side of Eq. (2) for the molecular flux of particles describes Brownian (molecular) diffusion of particles, the second term accounts for the molecular flux

of particles, which is driven by the fluid temperature gradient $\mathbf{V}T$ (thermophoresis for particles or molecular thermal diffusion for gases), and the third term determines the molecular flux of particles, which is driven by the fluid pressure gradient $\mathbf{V}P$ (molecular barodiffusion). Here, D is the coefficient of the Brownian diffusion, $k_t \propto n$ is the thermal diffusion ratio, Dk_t is the coefficient of thermal diffusion, $k_p \propto n$ is the barodiffusion ratio, and Dk_p is the coefficient of barodiffusion.

In a turbulent flow, large-scale dynamics of particles is determined by the equation for the mean particle number density $\bar{n}(t, \mathbf{r})$

$$\frac{\partial \bar{n}}{\partial t} + \mathbf{V} \cdot (\bar{n} \bar{\mathbf{U}}_p) = -\mathbf{V} \cdot (\bar{\mathbf{J}}_T + \bar{\mathbf{J}}_M), \quad (3)$$

where $\bar{\mathbf{U}}_p$ is the mean particle velocity, $\bar{\mathbf{J}}_M$ is the averaged molecular flux of particles,

$$\bar{\mathbf{J}}_M = -D \left[\mathbf{V}\bar{n} + k_t \frac{\mathbf{V}\bar{T}}{\bar{T}} + k_p \frac{\mathbf{V}\bar{P}}{\bar{P}} \right], \quad (4)$$

\bar{T} and \bar{P} are the mean fluid temperature and pressure, respectively, and $\bar{\mathbf{J}}_T$ is the turbulent flux of particles,^{22,23}

$$\bar{\mathbf{J}}_T = -D_T \left[\mathbf{V}\bar{n} + k_T \frac{\mathbf{V}\bar{T}}{\bar{T}} + k_p \frac{\mathbf{V}\bar{P}}{\bar{P}} \right]. \quad (5)$$

Here, D_T is the coefficient of turbulent diffusion, $k_T = \bar{n} \alpha(d, Re, \bar{T})$ can be interpreted as the turbulent thermal diffusion ratio, $D_T k_T$ is the coefficient of turbulent thermal diffusion, $k_p = -\bar{n}$ can be interpreted as the turbulent barodiffusion ratio, $D_T k_p$ is the coefficient of turbulent barodiffusion, and $\alpha(d, Re, \bar{T})$ is the function that depends on the particle diameter, the Reynolds number, and the mean fluid temperature.²⁸

The physics of the effect of turbulent thermal diffusion for solid particles is as follows: $\rho_p \gg \rho$,^{22,23} where ρ_p is the material density of the particles. The inertia causes particles inside the turbulent eddies to drift out to the boundary regions between eddies due to the centrifugal inertial force. Indeed, for large Péclet numbers, when molecular diffusion of particles in Eq. (1) can be neglected, we obtain that $\mathbf{V} \cdot \mathbf{U}_p \approx -n^{-1} dn/dt$. On the other hand, for inertial particles, $\mathbf{V} \cdot \mathbf{U}_p = (\tau_p/\rho) \mathbf{V}^2 P$.²² Therefore, in regions with maximum fluid pressure fluctuations (where $\mathbf{V}^2 P < 0$), there is accumulation of inertial particles, i.e., $dn'/dt \propto -\bar{n} (\tau_p/\bar{\rho}) \mathbf{V}^2 P > 0$. These regions have low vorticity and high strain rate. Here, n' and p are fluctuations of the particle number density and fluid pressure, respectively, and $\bar{\rho}$ is the mean density of the surrounding fluid. Similarly, there is an outflow of inertial particles from regions with minimum fluid pressure fluctuations.

In homogeneous and isotropic turbulence with a zero gradient of the mean temperature, there is no preferential direction, so that there is no large-scale effect of particle accumulation, and the pressure (temperature) of the surrounding fluid is not correlated with the turbulent velocity field. The only non-zero correlation is $\langle (\mathbf{u} \cdot \mathbf{V})p \rangle$, which contributes to the flux of the turbulent kinetic energy density.

In temperature-stratified turbulence, fluctuations of fluid temperature θ and velocity \mathbf{u} are correlated due to a non-zero turbulent heat flux, $\langle \theta \mathbf{u} \rangle \neq \mathbf{0}$. Fluctuations of temperature cause pressure fluctuations, which result in fluctuations of the number density of particles. Note that in the mechanism of turbulent thermal diffusion, only

pressure fluctuations that are correlated with velocity fluctuations due to a non-zero turbulent heat flux play a crucial role. An increase of the fluid pressure fluctuations is accompanied by an accumulation of particles, and the direction of the mean flux of particles coincides with that of the turbulent heat flux. The turbulent flux of particles is directed to the minimum of the mean temperature, and the particles tend to be accumulated in this region.¹⁴

The similar effect of accumulation of particles in the vicinity of the mean temperature minimum and the formation of inhomogeneous spatial distributions of the mean particle number density exists also for non-inertial particles or gaseous admixtures in turbulent compressible flows.^{23,29,34} Compressibility in a low-Mach-number stratified turbulent fluid flow [with $\mathbf{V} \cdot \mathbf{u} \approx -(\mathbf{u} \cdot \nabla \bar{\rho})/\bar{\rho} \neq 0$] causes an additional non-diffusive component of the turbulent flux of non-inertial particles or gases and results in the formation of large-scale inhomogeneous structures in spatial distributions of non-inertial particles. In a temperature stratified turbulence, the preferential concentration of particles caused by turbulent thermal diffusion can occur in the vicinity of the minimum of the mean temperature. The latter effect is caused by the compressibility of the turbulent fluid flow [$\mathbf{V} \cdot \mathbf{u} \propto (\mathbf{u} \cdot \nabla \bar{T})/\bar{T} \neq 0$]. This effect plays an important role in the dynamics of gaseous pollutants in the stratified atmospheric turbulence.

III. SETUP FOR MEAN-FIELD NUMERICAL SIMULATIONS

For better understanding of the experimental results obtained in this study, we perform one-dimensional mean-field numerical simulations of turbulent transport of nanoparticles for the conditions pertinent to the laboratory experiments. In particular, we study the evolution of the mean number density of nanoparticles, $\bar{n}(t, z)$, by solving numerically the evolutionary equation for the mean number density of nanoparticles

$$\frac{\partial \bar{n}}{\partial t} + \mathbf{V}_z \left[\left(V_z^{(\text{eff})} + V_z^{(\text{tp})} \right) \bar{n} - (D + D_T) \nabla_z \bar{n} \right] = 0. \quad (6)$$

This equation takes into account the total transport effective velocity $\mathbf{V}^{(\text{eff})} + \mathbf{V}^{(\text{tp})}$ due to turbulent thermal diffusion and thermophoresis, where $\mathbf{V}^{(\text{eff})}$ is the effective pumping velocity caused by turbulent thermal diffusion and $\mathbf{V}^{(\text{tp})}$ is the thermophoretic velocity (see below). This equation also takes into account the total particle diffusion $D + D_T$, where D is the coefficient of the Brownian diffusion, $D_T = u_0 \ell_0/3$ is the coefficient of turbulent diffusion, and u_0 is the characteristic turbulent velocity at the integral turbulence scale ℓ_0 . In one-dimensional mean-field numerical simulations, we have not taken into account the mean velocity field of the large-scale circulation produced in a small-scale convective turbulence.

Turbulent thermal diffusion is described in terms of the effective pumping velocity $\mathbf{V}^{(\text{eff})}$ resulting in the non-diffusive turbulent particle flux, $\bar{n} \mathbf{V}^{(\text{eff})}$. The effective pumping velocity caused by turbulent thermal diffusion of nanoparticles is given by

$$\mathbf{V}^{(\text{eff})} = -D_T \alpha(d, \text{Kn}, \text{Re}) \frac{\nabla \bar{T}}{\bar{T}}, \quad (7)$$

where

$$\alpha(d, \text{Kn}, \text{Re}, \bar{T}) = 1 + \frac{\tau_p(d, \text{Kn})}{\tau_0} \text{Re}^{1/4} \ln(\text{Re}) \left(\frac{L_{\text{eff}}}{\ell_0} \right), \quad (8)$$

(see Refs. 19, 35, and 47), where $L_{\text{eff}} = 2c_s^2 \tau_\eta^{3/2}/3\nu^{1/2}$ is the effective length scale, c_s is the sound speed, $\tau_p = m_p C_c/(3\pi\rho \nu d)$ is the Stokes time for nanoparticles, and $C_c = 1 + \text{Kn}[1.257 + 0.4 \exp(-1.1\text{Kn})]$ is the slip correction factor.⁴⁸ For instance, $C_c = 4.95$ for $d = 50$ nm, $C_c = 3.7$ for $d = 70$ nm, and $C_c = 2.85$ for $d = 100$ nm.¹¹

In turbulent flows, at the vicinity of the boundaries where the intensity of velocity fluctuations drastically decreases, the molecular effects (e.g., molecular diffusion and thermophoresis) become more important than the turbulent effects. The thermophoretic velocity can be estimated as $V^{(\text{tp})} = -f_{\text{tp}} \nu \nabla \bar{T}/\bar{T}$, where f_{tp} is a function of the Knudsen number, the particle size, and the ratio of the heat conductivities of the particle and the fluid. For small particles (i.e., for large Knudsen numbers, $\text{Kn} \gg 1$), the coefficient $f_{\text{tp}} = 3/4$ for mirror rebound of the gas molecules from the particles and $f_{\text{tp}} = 1/2$ for diffuse evaporation of the molecules when they “forget” the direction and value of their velocity prior to the impact.⁴⁹ Different aspects related to molecular effects have been studied in a number of publications.^{50–53}

In mean-field numerical simulations, we use the following boundary conditions:

- at the bottom boundary ($z = 0$), the total flux of particles,

$$F_z^{(n)} = \left(V_z^{(\text{eff})} + V_z^{(\text{tp})} \right) \bar{n} - (D + D_T) \nabla_z \bar{n}, \quad (9)$$

vanishes;

- at the upper boundary ($z = L_z$), the vertical gradient of the mean number density of nanoparticles $\nabla_z \bar{n}$ vanishes. The latter condition implies that all particles in the vicinity of the cold wall of the chamber (the upper boundary) are trapped due to adhesion of particles at the wall.

The total transport effective velocity $\mathbf{V}^{(\text{eff})} + \mathbf{V}^{(\text{tp})}$ caused by turbulent thermal diffusion and thermophoresis depends on the vertical profile of the mean temperature. We determine semi-analytically the vertical profile of the mean temperature. To this end, we take into account that the vertical component of the turbulent heat flux is $F_z = \langle u_z \theta \rangle = -\kappa_T \nabla_z \bar{T}$, where $\kappa_T = \ell_z u_z^{(\text{rms})} = (2\ell_z^4 \beta F_z)^{1/3}$ is the turbulent heat conductivity, $\beta = g/T_*$ is the buoyancy parameter, g is the gravity acceleration, T_* is the characteristic temperature in the basic reference state, and ℓ_z is the vertical integral turbulent scale. We take into account that in convective turbulence, the characteristic vertical turbulent velocity is $u_z^{(\text{rms})} = (2\ell_z \beta F_z)^{1/3}$. The latter equation follows from the steady-state solution of the budget equation for the turbulent kinetic energy, which allows us to relate the turbulent velocity with the turbulent heat flux. Next, we use the following model for the vertical integral length scale: in the core flow (for $z_* \leq z \leq L_z - z_*$), the vertical integral length is $\ell_z = \ell_0$; and near the bottom and top boundaries where the intensity of turbulence vanishes, the vertical integral length is $\ell_z = \ell_0 \phi(z)$. Here, L_z is the thickness of the convective layer (the vertical height of the chamber), $z_* = \epsilon L_z$ with $\epsilon \ll 1$, and $\phi(z)$ is the rapidly decreasing smooth function that varies from 1 to 0.

At the vicinity of the boundaries, the molecular diffusion of the mean temperature is taking into account, so that the total vertical heat flux $F_z^{(\text{tot})}$ is the sum of turbulent, $-\kappa_T \nabla_z \bar{T}$, and molecular, $-\kappa \nabla_z \bar{T}$, vertical heat fluxes, i.e., $F_z^{(\text{tot})} = -(\kappa_T + \kappa) \nabla_z \bar{T}$, where κ is the

molecular temperature diffusivity. The latter equation can be reduced to a cubic equation $N M^3 + M^2 - N = 0$ for $M = (F_z/F_z^{(tot)})^{1/3}$, where $N = \kappa^{-1} (2\ell_z^4 \beta F_z^{(tot)})^{1/3}$. The numerical solution of this cubic equation allows us to obtain the vertical profile for the mean temperature. This vertical profile of the mean temperature is used to determine the total transport effective velocity $V^{(eff)} + V^{(tp)}$ caused by turbulent thermal diffusion and thermophoresis in mean-field numerical simulations of nanoparticles in convective turbulence for the conditions pertinent to the laboratory experiments. The numerical simulations are performed using Matlab. The numerical results will be compared with the experimental results (see Sec. IV).

IV. EXPERIMENTAL SETUP

We conduct various sets of experiments in a temperature stratified convective turbulence. The experimental setup with an isolated chamber is designed for measurements of spatial distributions of the

fluid temperature and the number density of nanoparticles in turbulent convection (see Figs. 1 and 2). The chamber is fully isolated using high-quality glass, and there is also control humidity in the chamber.

The experiments are conducted with air as the working fluid in a rectangular chamber with dimensions $L_x \times L_y \times L_z$, where $L_x = L_z = 20$ cm, $L_y = 50$ cm, and the z axis is in the vertical direction (see Fig. 1, bottom panel). A vertical mean temperature gradient in the turbulent air flow is formed by attaching two aluminum heat exchangers to the bottom and top walls of the test section (a heated bottom and a cooled top wall of the chamber). A thickness of the massive aluminum heat exchangers is 2 cm. The top plate is a bottom wall of the tank with cooling water. Cold water is pumped into the cooling system through two inlets and flows out through two outlets located at the sidewall of the cooling system. The bottom plate is attached to the electrical heater with wire tightly laid in the grooves milled in the aluminum plate and provided uniform heating. Energy supplied to the heater is varied in order to obtain necessary temperature difference between the heater and cooler. The characteristic time of the heater is approximately 180 min that stabilizes the applied temperature during measurements.

The temperature field is measured with a temperature probe equipped with 11 E-thermocouples (with the diameter of 0.13 mm and the sensitivity of $\approx 65 \mu V/K$) attached to a rod with a diameter of 4 mm (see Fig. 1, bottom panel). The spacing between thermocouples along the rod can be changed from 10 to 20 mm. Each thermocouple is inserted into a 1 mm diameter and 45 mm long case. A tip of a

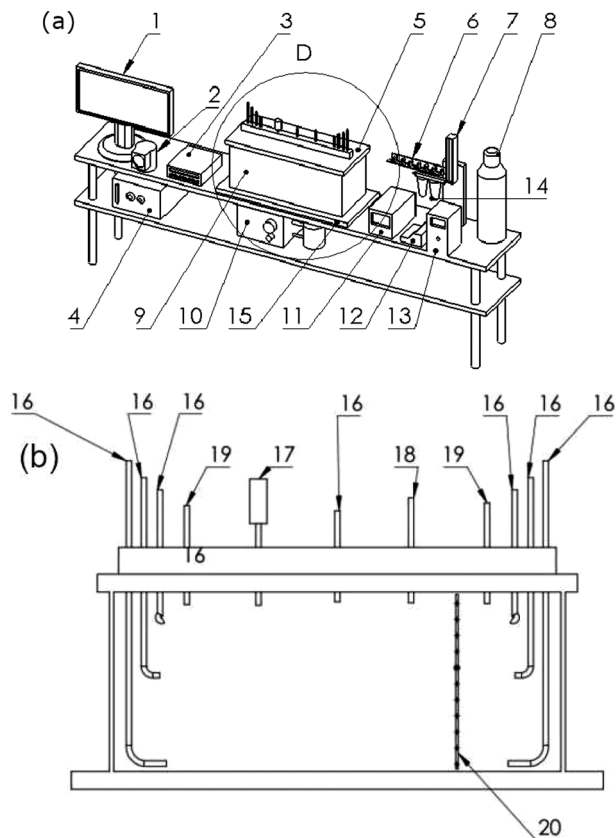


FIG. 1. A scheme of the experimental setup: (a). Upper panel: (1) display; (2) pressure measurements device; (3) data collection for temperature and humidity measurements; (4) computer; (5) cooler plate; (6) and (7) controllers for nanoparticle number density measurements; (8) container for CO₂ for nanoparticles generator; (9) chamber (see also the bottom panel); (10) cooling system; (11) nanoparticles generator; (12) spray for nanoparticles generator; (13) condensation particle counter; (14) air quality controller nanoparticles generator; (15) heating system. (b). Bottom panel: (16) probes for nanoparticle number density measurements; (17) probe for humidity measurements; (18) probe for pressure measurements; (19) air supply tube; (20) probes for temperature measurements.

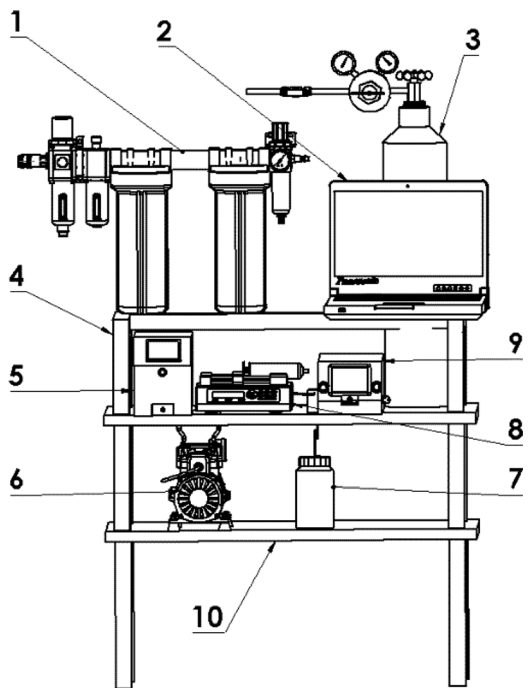


FIG. 2. A scheme of the experimental setup: (1) air filter and dryer for particles generator; (2) display; (3) gas cylinder CO₂ for particles generator; (4) frame; (5) particles counter; (6) vacuum pump of particles counter; (7) butanol waste container (drain balun of counter); (8) particles supply pump; (9) particles generator; (10) frame.

thermocouple protruded at the length of 15 mm out of the case. Thermocouples of type *E* are used for the temperature measurements in the core flow, while thermocouples of type *K* are used for temperature measurements at the heater and the cooler. All thermocouples are built by a manufacturer. Calibrations of all *E*-thermocouples in the temperature probe are performed for three experiments with boiled water ($T = 373$ K), the cold water with ice ($T = 273$ K), and water with intermediate temperature ($T = 296$ K). Comparisons is performed using a precision temperature measurement manufactured device.

The temperature is measured for 11 rod positions with 10–20 mm intervals in the horizontal direction. A sequence of 240 temperature readings for every thermocouple at every rod position is recorded and processed. We measure the temperature field in many locations. Performing direct continuous measurements of the temperatures at the cooled top surface and at the heated bottom surface and using a standard device for supporting constant temperature difference ΔT between the top and bottom surfaces (Contact voltage regulator TDGC-2K), we control the constant temperature difference ΔT during the experiments.

Similar measurement techniques and data processing procedure have been used by us previously in the experimental study of different aspects of turbulent convection and stably stratified turbulence,^{54–57} investigations of turbulent thermal diffusion^{22–25} of micrometer-size particles in the oscillating grid turbulence^{28,30–32} and in turbulence produced by the multi-fan generator,³³ and investigations of small-scale particle clustering^{47,58,59} in the oscillating grid turbulence.⁶⁰

To study turbulent thermal diffusion in the experiments, we use 70 nm nanoparticles produced by an advanced electrospray aerosol generator (Model 3482). To determine the number density of nanoparticles, we use a condensation particle counter (Model 3750). We conduct experiments for different temperature differences (from $\Delta T = 29$ up to $\Delta T = 61$ K) between the top and bottom walls as well as for isothermal flow. The particle number density measurements are performed for three heights z and two horizontal coordinates y .

V. RESULTS

Let us discuss the obtained results. In Fig. 3, we show the patterns of the mean temperature field \bar{T} in the yz plane obtained in the laboratory experiments for different temperature differences ΔT between the bottom and upper walls of the chamber: $\Delta T = 29$ K (upper panel), $\Delta T = 44$ K (middle panel), and $\Delta T = 61$ K (bottom panel). Figure 3 indicates that there are two large-scale circulations in the experiments for $\Delta T = 29$ and $\Delta T = 44$ K and one large-scale circulation for $\Delta T = 61$ K. The Rayleigh number $Ra = \alpha_* g L_z^3 \Delta T / (\nu \kappa)$ in the experiments varies in the interval $Ra = (0.61 - 1.23) \times 10^8$ depending on the different temperature differences ΔT between the bottom and upper walls of the chamber, where α_* is the thermal expansion coefficient and L_z is the height of the chamber.

In the present study, we have not performed measurements of the velocity field. The velocity field in turbulent convection in a similar experimental setup has been investigated in our previous study,⁵⁴ where we have determined the mean and turbulent velocity fields, the integral scales of turbulence in the horizontal and vertical directions, the rates of energy dissipation and production in the convective turbulence, and the dependencies of these turbulent parameters on the values of the temperature difference between the bottom and top walls of

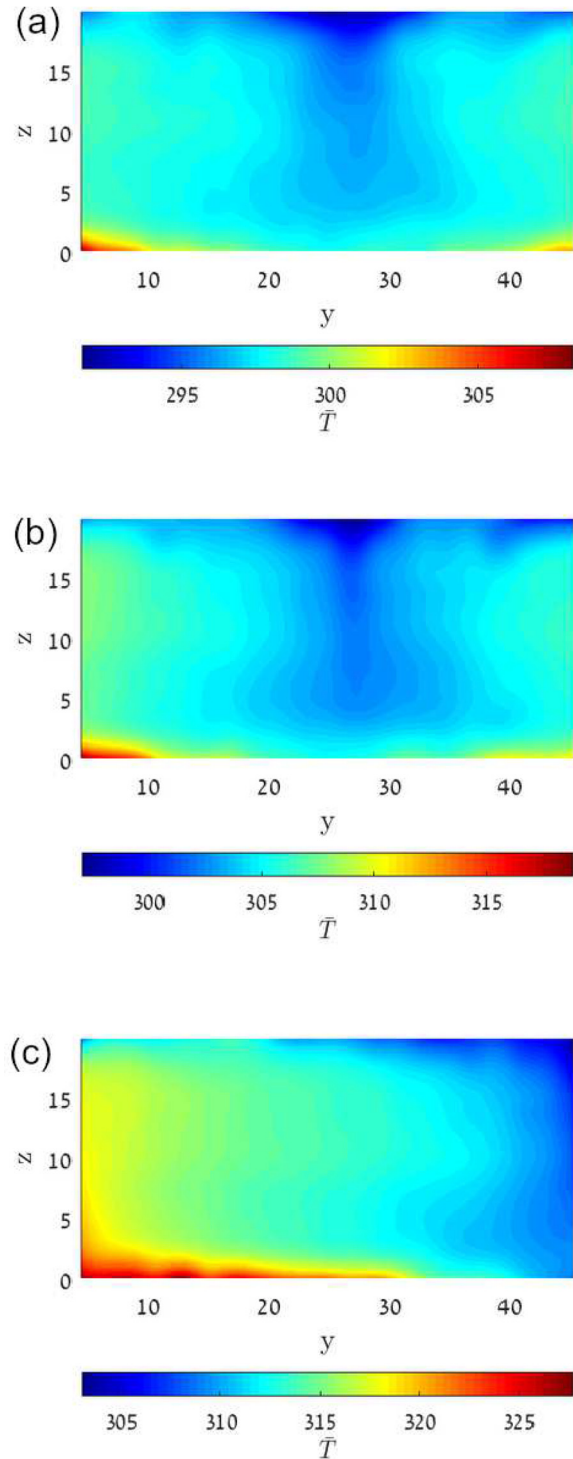


FIG. 3. Patterns of the mean temperature field \bar{T} in the yz plane obtained in the laboratory experiments for different temperature differences ΔT between the bottom and upper walls of the chamber: (a) $\Delta T = 29$ K (upper panel); (b) $\Delta T = 44$ K (middle panel); (c) $\Delta T = 61$ K (bottom panel). The coordinates are measured in cm, and the temperature is measured in K.

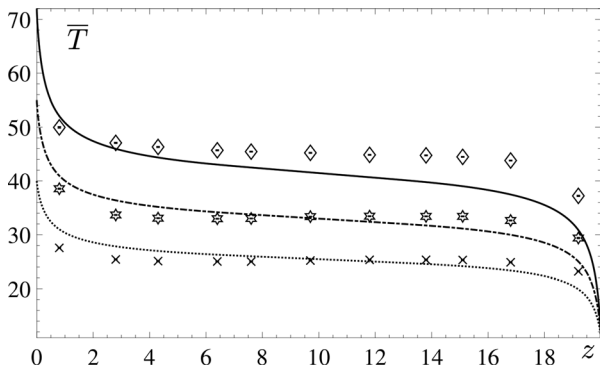


FIG. 4. Comparison of vertical profiles of the mean temperature \bar{T} obtained in the laboratory experiments for different temperature differences ΔT between the bottom and upper walls of the chamber: $\Delta T = 29$ K (slanting crosses); $\Delta T = 44$ K (stars); $\Delta T = 61$ K (diamonds); and in the semi-analytical mean-field calculations: $\Delta T = 29$ K (dotted line); $\Delta T = 44$ K (dashed line); $\Delta T = 61$ K (solid line). The coordinate z is measured in cm and the mean temperature in C.

the chamber. For instance, the integral turbulence scales in the chamber with convective turbulence are $\ell_x = \ell_z = 3$ cm, $\ell_y = 5$ cm, and the characteristic vertical turbulent velocity is $u_z = 5$ cm/s at $\Delta T = 60$ K that depends on ΔT as $u_z \propto (\Delta T)^{1/2}$.⁵⁴

In Figs. 4 and 5, we also plot vertical profiles of the mean temperature \bar{T} and the vertical gradient $\nabla_z \bar{T}$ of the mean temperature obtained in the laboratory experiments for different temperature differences ΔT between the bottom and upper walls of the chamber. These profiles of the mean temperature \bar{T} are compared with the results of the semi-analytical mean-field calculations described at the end of Sec. II. Figures 4 and 5 show that there is qualitative agreement between the modeling and experimental results. In general, the strong temperature gradient is located near the walls of the chamber, while inside the large-scale circulations, the vertical gradient $\nabla_z \bar{T}$ of the mean temperature is much weaker. The main reason for the deviations of the modeling and experimental results for the temperature field is

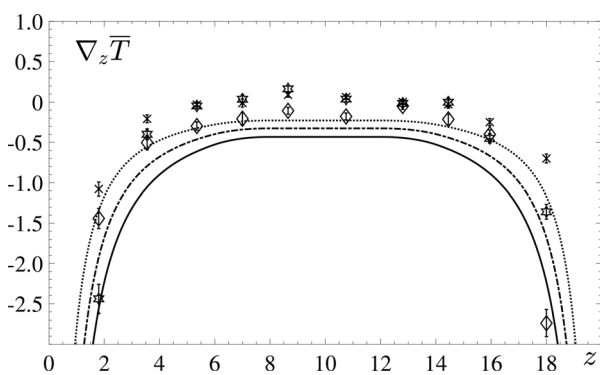


FIG. 5. Comparison of vertical profiles of the vertical mean temperature gradient $\nabla_z \bar{T}$ obtained in the laboratory experiments for different temperature differences ΔT between the bottom and upper walls of the chamber: $\Delta T = 29$ K (slanting crosses); $\Delta T = 44$ K (stars); $\Delta T = 61$ K (diamonds); and in the semi-analytical mean-field calculations: $\Delta T = 29$ K (dotted line); $\Delta T = 44$ K (dashed line); $\Delta T = 61$ K (solid line). The coordinate z is measured in cm, and the mean temperature gradient $\nabla_z \bar{T}$ is measured in K/cm.

that in the one-dimensional semi-analytical calculations of the vertical mean temperature distribution, we have not taken into account the mean velocity field of the large-scale circulation. We have checked a particular form of the decreasing smooth function $\phi(z)$ that describes the spatial vertical profile of the integral turbulence scale in the region, where the turbulent intensity strongly decreases and weakly affects the mean temperature distribution. Note also that we have not performed temperature measurements in the vicinity of the wall but measure temperature at the heat exchangers and in the core flow.

Measurements of the number density of nanoparticles allow us to determine the time evolution of the normalized mean number density $\bar{n}(t)/\bar{n}_0$ of nanoparticles obtained in the laboratory experiments for different temperature differences ΔT between the bottom and upper walls of the chamber (see Fig. 6). Here, $\bar{n}(t) = L_z^{-1} \int_0^{L_z} \bar{n}(t, z) dz$ is the mean number density of nanoparticles averaged over the vertical coordinate z and $\bar{n}_0 = \bar{n}(t = 0)$. Inspection of Fig. 6 shows that in the experiments with turbulent convection with different temperature differences between the bottom and top walls of the chamber, the mean number density of nanoparticles decreases exponentially in time. The characteristic decay time of the mean number density of nanoparticles varies from 12.8 min for the temperature difference $\Delta T = 61$ K to 16.3 min for $\Delta T = 44$ K and to 24 min for $\Delta T = 29$ K.

We also perform comparison of the obtained experimental results with the results of the mean-field numerical simulations of transport of nanoparticles, which accounts for molecular and turbulent effects for the conditions pertinent to the laboratory experiments. The numerical setup is described in Sec. II. As follows from Fig. 6, the obtained numerical results related to the time evolution of the normalized mean number density of particles $\bar{n}(t)/\bar{n}_0$ are in agreement with the results of the laboratory experiments.

In Fig. 7, we show the time evolution of the ratios of the mean number densities of nanoparticles $\bar{n}_{\text{bottom}}/\bar{n}_{\text{top}}$ and $\bar{n}_{\text{middle}}/\bar{n}_{\text{top}}$ obtained in the laboratory experiments for the temperature difference $\Delta T = 61$ K between the bottom and top walls of the chamber, where \bar{n}_{top} , \bar{n}_{bottom} , and \bar{n}_{middle} are the mean number densities of nanoparticles measured in the vicinity of the top, bottom, and middle parts of

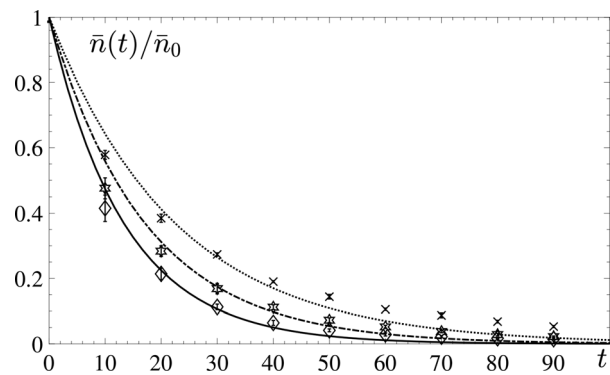


FIG. 6. Comparison of the time evolution of the normalized mean number density of nanoparticles $\bar{n}(t)/\bar{n}_0$ obtained in the laboratory experiments for different temperature differences ΔT between the bottom and upper walls of the chamber: $\Delta T = 29$ K (slanting crosses); $\Delta T = 44$ K (stars); $\Delta T = 61$ K (diamonds); and in the mean-field simulations: $\Delta T = 29$ K (dotted line); $\Delta T = 44$ K (dashed line); $\Delta T = 61$ K (solid line). Here, $\bar{n}(t) = L_z^{-1} \int_0^{L_z} \bar{n}(t, z) dz$ and $\bar{n}_0 = \bar{n}(t = 0)$. The time is measured in minutes.

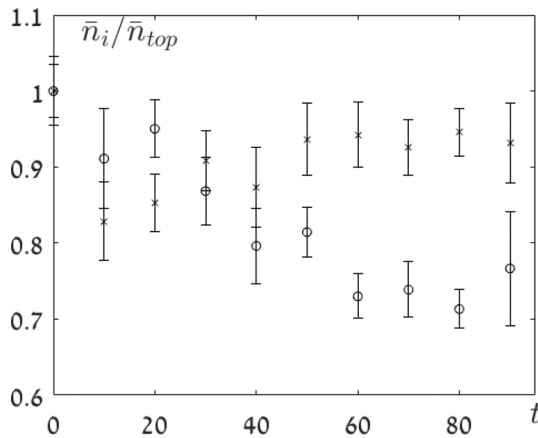


FIG. 7. The time evolution of the ratios of the mean number densities of nanoparticles $\bar{n}_{bottom}/\bar{n}_{top}$ (slanting crosses) and $\bar{n}_{middle}/\bar{n}_{top}$ (circles) obtained in the laboratory experiments for the temperature difference $\Delta T = 61$ K between the bottom and top walls of the chamber, where \bar{n}_{top} , $\bar{n}_i = \bar{n}_{bottom}$, and $\bar{n}_i = \bar{n}_{middle}$ are the mean number densities of nanoparticles measured at the top, bottom, and middle parts of the chamber, respectively. The time is measured in minutes.

the chamber, respectively. Figure 7 demonstrates that the distribution of the mean number density of nanoparticles is inhomogeneous. In particular, the maximum mean number density of nanoparticles is located near the top cold wall of the chamber, i.e., for $t > 0$, the ratios $\bar{n}_{bottom}/\bar{n}_{top}$ and $\bar{n}_{middle}/\bar{n}_{top}$ are always less than 1.

Let us estimate the effective pumping velocity caused by turbulent thermal diffusion of nanoparticles, the velocity due to the thermophoresis, and the terminal fall velocity. The effective pumping velocity caused by turbulent thermal diffusion of nanoparticles having the diameter $d = 70$ nm is 7×10^{-2} cm/s, where we use Eqs. (7) and (8). We also take into account that the value of the gradient of the mean temperature measured in the core flow at $3 \leq z \leq 17$ cm is $\nabla_z \bar{T} = 0.4$ K/cm (see Fig. 5). In the core flow, the turbulent effects (turbulent thermal diffusion and turbulent diffusion) are dominant in comparison with the molecular effects. Now we estimate the terminal fall velocity $V_g = \tau_p g$ of nanoparticles due to the gravity field, that is about $V_g = 3 \times 10^{-5}$ cm/s, where $\tau_p = 3 \times 10^{-8}$ s is the Stokes time for nanoparticles with the diameter $d = 70$ nm. The velocity due to the thermophoresis in the vicinity of the cold wall is about $V^{(tp)} = 1.2 \times 10^{-3}$ cm/s at $z = 1.6$ cm, where the gradient of the mean temperature is 3 K/cm.

VI. DISCUSSION AND CONCLUSIONS

We have performed different sets of experiments with turbulent convection to study the turbulent transport of nanoparticles. The temperature field has been measured with a temperature probe equipped with 11 E-thermocouples. To determine the number density of nanoparticles, we used a condensation particle counter. Nanoparticles of 70 nm in diameter are produced by the advanced electrospray aerosol generator. We measure the number density of nanoparticles as a function of time in three locations in vertical directions. In the different experiments with turbulent convection with the temperature difference between the bottom and top walls of the chamber ΔT varying between $\Delta T = 29$ and $\Delta T = 61$ K, it has been shown that the mean

number density of nanoparticles decreases exponentially in time. For instance, the characteristic decay time of the mean number density of nanoparticles varies from 12.8 min for the temperature difference between the bottom and top walls of the chamber $\Delta T = 61$ K to 16.3 min for $\Delta T = 44$ K and to 24 min for $\Delta T = 29$ K. The main reasons for this effect are as follows:

- The large-scale circulations in convective turbulence in the updrafts and the effective pumping velocity due to turbulent thermal diffusion in the core flow result in the drift of nanoparticles to the cold wall of the chamber. Turbulent thermal diffusion is a turbulent effect, and it vanishes near the walls whereby the intensity of turbulence tends to zero.
- In the vicinity of the walls, the molecular effects (the thermophoresis and adhesion of nanoparticles) play a crucial role in the particle accumulation at the cold wall of the chamber. The thermophoretic velocity is proportional to $-\nabla T$, and the mean temperature gradient is maximum in the vicinity of the walls. Therefore, the thermophoretic velocity finally causes the trapping of particles by the cold wall of the chamber.

We have also performed one-dimensional mean-field numerical simulations of the evolution of the mean number density of nanoparticles, which take into account turbulent and molecular effects. The molecular effects include the Brownian diffusion of nanoparticles, the thermophoresis, and the adhesion of nanoparticles at the cold surfaces. The turbulent effects are described by turbulent diffusion and turbulent thermal diffusion of nanoparticles. These simulations allow us to determine the time-dependence of the mean number density of nanoparticles and to find the characteristic decay time of the mean concentration of nanoparticles. The obtained numerical results are in agreement with the experimental results.

Several different mechanisms affect the particle transport. In the core flow, there are two alternative mechanisms of the vertical transport of nanoparticles to the vertical cold wall of the chamber: (i) turbulent thermal diffusion that causes drift of nanoparticles to the vertical cold wall of the chamber and (ii) the mean fluid velocity of the large-scale circulations in the updrafts. Our experiments in convective turbulence cannot give a certain answer, which mechanism is dominant.

In particular, the effective pumping velocity caused by turbulent thermal diffusion is the vertical velocity directed to the cold wall of the chamber. (It is proportional to $-\nabla T$.) This pumping velocity can cause an inhomogeneous distribution of nanoparticles, where particles tend to be accumulated in the vicinity of the cold wall of the chamber. On the other hand, the mean fluid velocity of the large-scale circulations causes mixing of nanoparticles in the chamber producing nearly homogeneous distribution of nanoparticles in the chamber. However, the mean fluid velocity in the updrafts inside the large-scale circulations can also cause the transport of nanoparticles to the vertical cold wall of the chamber.

Both mechanisms result in the transport of nanoparticles to the vertical cold wall of the chamber. The turbulent thermal diffusion acts in all core flow, while the mean fluid velocity of the large-scale circulations is effective in the vertical transport only in the updrafts, and the region occupied by the updrafts in the large-scale circulation is much smaller than the size of the large-scale circulation.

One-dimensional mean-field numerical simulations of the evolution of the mean number density of nanoparticles, which take into

account turbulent and molecular effects but do not take into account the three-dimensional large-scale circulations, have shown that the presence of both turbulent thermal diffusion and thermophoresis is already enough to explain the measured in the laboratory experiments characteristic times of the accumulation of nanoparticles in the vertical cold wall of the chamber.

Our previous experiments³² with micrometer-size particles in convective turbulence have shown that an additional source of turbulence by oscillating grids results in a destruction of the large-scale circulations. In this case, the turbulent thermal diffusion coefficient α for convective (unstably stratified) turbulence is the same as in the experiments with a stably stratified turbulence (with the heating upper wall and the cooling bottom wall of the chamber) performed for the same temperature difference ΔT between the bottom and top walls of the chamber and the same frequency of the grid oscillations.³²

Future experiments with nanoparticles in stably stratified turbulence, where there are no large-scale circulations, can demonstrate the importance of turbulent thermal diffusion for transport of nanoparticles. However, such experiments with nanoparticles in an isolated chamber require a source of turbulence, which does not destroy the isolation of the chamber. For instance, oscillating grid turbulence^{30–32} or multi-fan produced turbulence³³ cannot be used in the experiments with nanoparticles.

ACKNOWLEDGMENTS

This research was supported in part by the Israel Ministry of Science and Technology (Grant No. 3-16516).

AUTHOR DECLARATIONS

Conflict of Interest

The authors have no conflicts to disclose.

DATA AVAILABILITY

The data that support the findings of this study are available from the corresponding author upon reasonable request.

REFERENCES

- A. S. Monin and A. M. Yaglom, *Statistical Fluid Mechanics* (MIT Press, Cambridge, 1971), Vol. 1.
- A. S. Monin and A. M. Yaglom, *Statistical Fluid Mechanics* (MIT Press, Cambridge, 1975), Vol. 2.
- W. D. McComb, *The Physics of Fluid Turbulence* (Oxford Science Publications, Oxford, 1990).
- U. Frisch, *Turbulence: The Legacy of A. N. Kolmogorov* (Cambridge University Press, Cambridge, 1995).
- S. B. Pope, *Turbulent Flows* (Cambridge University Press, Cambridge, 2000).
- M. Lesieur, *Turbulence in Fluids* (Springer, Dordrecht, 2008).
- P. A. Davidson, *Turbulence in Rotating, Stratified and Electrically Conducting Fluids* (Cambridge University Press, Cambridge, 2013).
- G. T. Csanady, *Turbulent Diffusion in the Environment* (Reidel, Dordrecht, 1980).
- Y. B. Zeldovich, A. A. Ruzmaikin, and D. D. Sokoloff, *The Almighty Chance* (Word Scientific Publishing, Singapore, 1990).
- A. K. Blackadar, *Turbulence and Diffusion in the Atmosphere* (Springer, Berlin, 1997).
- J. H. Seinfeld and S. N. Pandis, *Atmospheric Chemistry and Physics. From Air Pollution to Climate Change*, 2nd ed. (John Wiley & Sons, NewYork, 2006).
- L. I. Zaichik, V. M. Alipchenkov, and E. G. Sinaiski, *Particles in Turbulent Flows* (John Wiley & Sons, NewYork, 2008).
- C. T. Crowe, J. D. Schwarzkopf, M. Sommerfeld, and Y. Tsuji, *Multiphase Flows With Droplets and Particles*, 2nd ed. (CRC Press LLC, NY, 2011).
- I. Rogachevskii, *Introduction to Turbulent Transport of Particles, Temperature and Magnetic Fields* (Cambridge University Press, Cambridge, 2021).
- G. I. Taylor, "Diffusion by continuous movements," *Proc. London Math. Soc.* **s2-20**, 196 (1922).
- M. Caporali, F. Tampieri, F. Trombetti, and O. Vittori, "Transfer of particles in nonisotropic air turbulence," *J. Atmos. Sci.* **32**, 565 (1975).
- M. Reeks, "The transport of discrete particle in inhomogeneous turbulence," *J. Aerosol Sci.* **14**, 729 (1983).
- A. Guha, "A unified Eulerian theory of turbulent deposition to smooth and rough surfaces," *J. Aerosol Sci.* **28**, 1517 (1997).
- T. Elperin, N. Kleeorin, and I. Rogachevskii, "Formation of inhomogeneities in two-phase low-Mach-number compressible turbulent fluid flows," *Int. J. Multiphase Flow* **24**, 1163 (1999).
- A. Guha, "Transport and deposition of particles in turbulent and laminar flow," *Annu. Rev. Fluid Mech.* **40**, 311 (2008).
- D. Mitra, N. E. L. Haugen, and I. Rogachevskii, "Turbophoresis in forced inhomogeneous turbulence," *Europ. Phys. J. Plus* **133**, 35 (2018).
- T. Elperin, N. Kleeorin, and I. Rogachevskii, "Turbulent thermal diffusion of small inertial particles," *Phys. Rev. Lett.* **76**, 224 (1996).
- T. Elperin, N. Kleeorin, and I. Rogachevskii, "Turbulent barodiffusion, turbulent thermal diffusion and large-scale instability in gases," *Phys. Rev. E* **55**, 2713 (1997).
- T. Elperin, N. Kleeorin, I. Rogachevskii, and D. Sokoloff, "Passive scalar transport in a random flow with a finite renewal time: Mean-field equations," *Phys. Rev. E* **61**, 2617 (2000).
- T. Elperin, N. Kleeorin, I. Rogachevskii, and D. Sokoloff, "Mean-field theory for a passive scalar advected by a turbulent velocity field with a random renewal time," *Phys. Rev. E* **64**, 026304 (2001).
- R. V. R. Pandya and F. Mashayek, "Turbulent thermal diffusion and barodiffusion of passive scalar and dispersed phase of particles in turbulent flows," *Phys. Rev. Lett.* **88**, 044501 (2002).
- M. W. Reeks, "On model equations for particle dispersion in inhomogeneous turbulence," *Int. J. Multiphase Flow* **31**, 93 (2005).
- G. Amir, N. Bar, A. Eidelman, T. Elperin, N. Kleeorin, and I. Rogachevskii, "Turbulent thermal diffusion in strongly stratified turbulence: Theory and experiments," *Phys. Rev. Fluids* **2**, 064605 (2017).
- I. Rogachevskii, N. Kleeorin, and A. Brandenburg, "Compressibility in turbulent magnetohydrodynamics and passive scalar transport: Mean-field theory," *J. Plasma Phys.* **84**, 735840502 (2018).
- J. Buchholz, A. Eidelman, T. Elperin, G. Grünefeld, N. Kleeorin, A. Krein, and I. Rogachevskii, "Experimental study of turbulent thermal diffusion in oscillating grids turbulence," *Exp. Fluids* **36**, 879 (2004).
- A. Eidelman, T. Elperin, N. Kleeorin, A. Krein, I. Rogachevskii, J. Buchholz, and G. Grünefeld, "Turbulent thermal diffusion of aerosols in geophysics and in laboratory experiments," *Nonlinear Processes Geophys.* **11**, 343 (2004).
- A. Eidelman, T. Elperin, N. Kleeorin, A. Markovich, and I. Rogachevskii, "Experimental detection of turbulent thermal diffusion of aerosols in non-isothermal flows," *Nonlinear Processes Geophys.* **13**, 109 (2006).
- A. Eidelman, T. Elperin, N. Kleeorin, I. Rogachevskii, and I. Sapir-Katirae, "Turbulent thermal diffusion in a multi-fan turbulence generator with the imposed mean temperature gradient," *Exp. Fluids* **40**, 744 (2006).
- N. E. L. Haugen, N. Kleeorin, I. Rogachevskii, and A. Brandenburg, "Detection of turbulent thermal diffusion of particles in numerical simulations," *Phys. Fluids* **24**, 075106 (2012).
- T. Elperin, N. Kleeorin, and I. Rogachevskii, "Mechanisms of formation of aerosol and gaseous inhomogeneities in the turbulent atmosphere," *Atmos. Res.* **53**, 117 (2000).
- M. Sofiev, V. Sofieva, T. Elperin, N. Kleeorin, I. Rogachevskii, and S. S. Zilitinkevich, "Turbulent diffusion and turbulent thermal diffusion of aerosols in stratified atmospheric flows," *J. Geophys. Res.* **114**, D18209, <https://doi.org/10.1029/2009JD011765> (2009).
- A. Hubbard, "Turbulent thermal diffusion: A way to concentrate dust in proto-planetary discs," *Mon. Not. R. Astron. Soc.* **456**, 3079–3089 (2016).

- ³⁸J. A. Eastman, S. R. Phillpot, S. U. S. Choi, and P. Keblinski, "Thermal transport in nanofluids," *Annu. Rev. Mater. Res.* **34**, 219–246 (2004).
- ³⁹C. Wang, S. K. Friedlander, and L. Mädler, "Nanoparticle aerosol science and technology: An overview," *Particuology* **3**, 243–254 (2005).
- ⁴⁰W. C. Williams, *Experimental and Theoretical Investigation of Transport Phenomena in Nanoparticle Colloids (Nanofluids)* (Institute of Technology, Massachusetts, 2007).
- ⁴¹W. Daungthongsuk and S. Wongwises, "A critical review of convective heat transfer in nanofluids," *Renewable Sustainable Energy Rev.* **11**, 797–817 (2007).
- ⁴²S. Kakac and A. Pramuanjaroenkij, "Review of convective heat transfer enhancement with nanofluid," *Int. J. Heat Mass Transfer* **52**, 3187–3196 (2009).
- ⁴³M. Yu and J. Lin, "Nanoparticle-laden flows via moment method: A review," *Int. J. Multiphase Flow* **36**, 144–151 (2010).
- ⁴⁴M. Lomascolo, G. Colangelo, M. Milanese, and A. de Risi, "Review of heat transfer in nanofluids: Conductive, convective and radiative experimental results," *Renewable Sustainable Energy Rev.* **43**, 1182–1198 (2015).
- ⁴⁵M. Raja, R. Vijayan, P. Dineshkumar, and M. Venkatesan, "Review on nanofluids characterization, heat transfer characteristics and applications," *Renewable Sustainable Energy Rev.* **64**, 163–173 (2016).
- ⁴⁶S. M. Vanaki, P. Ganesan, and H. A. Mohammed, "Numerical study of convective heat transfer of nanofluids: A review," *Renewable Sustainable Energy Rev.* **54**, 1212–1239 (2016).
- ⁴⁷T. Elperin, N. Kleeorin, M. A. Liberman, and I. Rogachevskii, "Tangling clustering instability for small particles in temperature stratified turbulence," *Phys. Fluids* **25**, 085104 (2013).
- ⁴⁸M. D. Allen and O. G. Raabe, "Reevaluation of Millikan's oil drop data for the motion of small particles in air," *J. Aerosol Sci.* **13**, 537–547 (1982).
- ⁴⁹B. V. Derjaguin, A. I. Storozhilova, and Y. I. Rabinovich, "Experimental verification of the theory of thermophoresis of aerosol particles," *J. Colloid Interface Sci.* **21**, 35–58 (1966).
- ⁵⁰L. Talbot, R. K. Cheng, R. W. Schefer, and D. R. Willis, "Thermophoresis of particles in a heated boundary layer," *J. Fluid Mech.* **101**, 737–758 (1980).
- ⁵¹C. He and G. Ahmadi, "Particle deposition with thermophoresis in laminar and turbulent duct flows," *Aerosol Sci. Technol.* **29**, 525–546 (1998).
- ⁵²G. Santachiara, F. Prodia, and C. Cornettia, "Experimental measurements on thermophoresis in the transition region," *Aerosol Sci. Technol.* **33**, 769–780 (2002).
- ⁵³A. E. Mensch and T. G. Cleary, "Measurements and predictions of thermophoretic soot deposition," *Intern. J. Heat Mass Transfer* **143**, 118444 (2019).
- ⁵⁴M. Bukai, A. Eidelman, T. Elperin, N. Kleeorin, I. Rogachevskii, and I. Sapir-Katiraie, "Effect of large-scale coherent structures on turbulent convection," *Phys. Rev. E* **79**, 066302 (2009).
- ⁵⁵M. Bukai, A. Eidelman, T. Elperin, N. Kleeorin, I. Rogachevskii, and I. Sapir-Katiraie, "Transition phenomena in unstably stratified turbulent flows," *Phys. Rev. E* **83**, 036302 (2011).
- ⁵⁶A. Eidelman, T. Elperin, I. Gluzman, N. Kleeorin, and I. Rogachevskii, "Experimental study of temperature fluctuations in forced stably stratified turbulent flows," *Phys. Fluids* **25**, 015111 (2013).
- ⁵⁷L. Barel, A. Eidelman, T. Elperin, G. Fleurov, N. Kleeorin, A. Levy, I. Rogachevskii, and O. Shildkrot, "Detection of standing internal gravity waves in experiments with convection over a wavy heated wall," *Phys. Fluids* **32**, 095105 (2020).
- ⁵⁸T. Elperin, N. Kleeorin, and I. Rogachevskii, "Self-excitation of fluctuations of inertial particles concentration in turbulent fluid flow," *Phys. Rev. Lett.* **77**, 5373 (1996).
- ⁵⁹T. Elperin, N. Kleeorin, V. L'vov, I. Rogachevskii, and D. Sokoloff, "Clustering instability of the spatial distribution of inertial particles in turbulent flows," *Phys. Rev. E* **66**, 036302 (2002).
- ⁶⁰A. Eidelman, T. Elperin, N. Kleeorin, B. Melnik, and I. Rogachevskii, "Tangling clustering of inertial particles in stably stratified turbulence," *Phys. Rev. E* **81**, 056313 (2010).